Supporting information for

Electrically Conductive [Fe_4S_4]-based Organometallic Polymers

Kentaro Kadota‡,[a] Tianyang Chen,[b] Eoghan Gormley,[a]
Christopher H. Hendon,[a] Mircea Dincă,[b] and Carl K. Brozek*[a]

[a]Department of Chemistry and Biochemistry, Materials Science Institute, University of Oregon, Eugene, OR 97403, United States

[b]Department of Chemistry, Massachusetts Institute of Technology, Cambridge, MA 02139, USA

‡ Current address: Institute for Integrated Cell-Material Sciences, Institute for Advanced Study, Kyoto University, Kyoto 606-8501, Japan

Table of Contents

Materials and general methods

All chemicals and solvents used in the syntheses were of reagent grade and used without any further purification. Iron chloride anhydrous ($FeCl_2$) and sulfur powder (S, sublimed 99%) were purchased from Strem Chemicals, Inc. Tetraphenylphosphonium chloride (PPh_4Cl, >98%), sodium hydride (NaH, 60%, dispersion in paraffin liquid), bromoethane (EtBr, >99%), and 1-bromopropane (PrBr, >98%) were purchased from TCI Co., Ltd. Sodium thiophenolate (NaSPh, 90%) and deuterium chloride (DCl, 20 wt% in D_2O) purchased from Acros Organics. Iodomethane (MeI, 99%) and sodium *tert*-butoxide (Na^tBuO, 97%) were purchased from Alfa Aesar. 1,2,4,5-benzenetetraamine tetrachloride (TAB, >95%) and 1-bromobutane (BuBr, 99%) were purchased from Sigma-Aldrich Co. Potassium carbonate anhydrous (K_2CO_3) was purchased from Fischer Science, Inc.

Powder X-ray diffraction (PXRD): Powder X-Ray diffraction with a Bruker D2 Phaser benchtop diffractometer (λ = 1.5418 Å). The sample was loaded into an airtight specimen holder under N_2 without exposure to the air.

Elemental analysis: CHN analysis under N_2 was performed by Midwest Microlab LLC.

Solution nuclear magnetic resonance (NMR): Acid-digested NMR spectrum was collected in 20% DCl/D_2O in DMSO-d_6 in the air, then filtered through cotton plugs prior to analysis with a Bruker Advance III-HD 600 NMR Spectrometer.

Fourier transform infrared (FT-IR): IR spectra were recorded on a Bruker Alpha II compact IR with an ATR attachment under N_2.

Scanning electron microscopy (SEM): Imaging was performed using a FEI Helios 600i instrument. SEM samples were prepared by dispersion of the powder sample onto the carbon tape substrates under N_2. The sample on the substrate was exposed to the air when transferred into the SEM instrument.

Pair distribution function (PDF) analysis: The powder sample was placed in a glass capillary, loaded in a Kapton capillary tube, and sealed with epoxy glue under N_2. Total X-ray scattering data were collected at λ = 0.2115 Å at 11-ID-B in Argonne national laboratory. The correction of the data for Compton scattering, multiplicative contributions, and Fourier transformation was performed with PDFgetX3.1.[1] The simulation of the PDF profile was performed on PDFGUI using the crystallographic data obtained from CIF files.[2]

Variable-temperature diffuse-reflectance UV-Vis (VT-DRUV-Vis) spectroscopy: VT-DRUV-vis spectroscopy was performed on a Perkin Elmer Lambda 1050 UV/Vis/NIR spectrometer, with a 150 mm InGaAs integrating sphere in the range of 2000-200 nm paired with a Harrick Scientific Praying Mantis Diffuse Reflection (DRP) accessory. A Harrick Scientific Low Temperature Reaction Chamber (CHC) that enabled introducing vacuum and heat to the sample was equipped with UV quartz. To ensure adequate absorbance, all samples were diluted under N_2 with ground $MgSO_4$ dried at 100 °C under vacuum.

Linear sweep voltammetry: Pressed pellets were prepared by compressing powders in a modified KBR pellet die set. The pellet press die set (0.402 cm^2) was modified with tinned copper wires affixed to both slight affixed to both sides with silver paint and epoxy. Electrical contacts were made by pressing a pellet with the modified die set comprised of stainless-steel circular ends serving as two electrode contacts. Direct-current (DC) conductivities were determined from the slopes of current-voltage (*I-V*) curves collected at the sweep rate of 10 mV s^{-1} with a GAMRY Instruments Interface 5000E potentiostat.

Solid-state cyclic voltammetry (CV): CV data were collected with a Biologic SP200. A 5 μL of DMF suspension of the sample (1.0 mg mL^{-1}) was drop-casted on CHI 104 3 mm diameter glassy carbon (GC) electrode, and dried at 25 °C under vacuum. CV experiments were performed in a standard three-electrode cell, with particle-coated GC as the working electrode, silver wire as a pseudo-reference electrode, and carbon cloth as a counter electrode. $LiPF_6$ or $TBAPF_6$ was used as a supporting electrolyte (0.1 M) in acetonitrile under N_2. CV scans were collected at rates of 10 mV s^{-1}.

Variable temperature diffuse-reflectance Fourier-transform infrared spectroscopy (DRIFTS): VT-DRIFTS experiment was performed on a Nicolet 6700 FT-IR spectrometer using a Transmission E.S.P. attachment paired with Harrick Scientific Praying Mantis Diffuse Reflection (DRP) accessory and MCT detector. A Harrick Scientific Low Temperature Reaction Chamber (CHC) that enabled introducing vacuum to the sample was equipped with 2 Harrick 15×2 mm potassium bromide windows. To maximize intensity, all samples were diluted with ground KBr dried at 100 °C under vacuum. Reflectance FTIR spectra were collected in the range of 4000–650 cm^{-1} with 2 cm^{-1} resolution and 32 scans.

Variable temperature electrical conductivity: The powder has been always kept in the glove box. The powder was pressed into a pellet (0.068 mm thickness measured) using a pellet die and a hydraulic press inside the glove box. The pellet was cut into a rectangular shape. The rectangular pellet was transferred onto a piece of sapphire, and four copper wires were attached to the pellet in the conventional four-contact probe configuration. The whole pellet was covered with grease to prevent air exposure when the device is taken out of the box. The device was transferred out of the box and onto an ETO puck of PPMS. The electrical contacts between device and ETO puck were made by soldering. The ETO puck was installed into the PPMS chamber for measurement. The resistance of the device was measured immediately after it was inside the PPMS chamber. The device was kept at 300 K under vacuum overnight to check the stability of the device, and the result is that the device is stable upon vacuum at 300 K. The resistance increased a little bit overnight. Then the device was cooled down first from 300 K to 200 K. The AC resistance was measured every 1 K with a cooling/heating rate of 3 K min^{-1}. The photos of device were taken before and after measurements, with an external ruler for the measurement of the dimension of the device.

Computational Details: Electronic structure calculations were performed on two $[Fe_4S_4]$ clusters – one with NHC ligands and an overall charge of +2 *e*, and one with BDT ligands and an overall charge of -2 *e*. The structures were relaxed using the GGA functional PBE, as implemented in the software FHI-aims, with a convergence criterion of 10^{-6} eV for the total energy of the structures and a force convergence criterion of $5x10^{-3}$ eV/Å. The structures were initialized with spin moments of 4 and -4 for two of the iron centers and 5 (-5) for the other two (these can be chosen without loss of generality due to symmetry) and allowed to relax with an enforced net spin moment of 0 for the overall structures. Finally, the frontier orbitals of each structure were visualized by extracting cube files from the calculation output files, and partial charges of the iron atoms and adjacent ligand atoms were examined through Mulliken analysis.

Synthesis of $(PPh_4)_2(Fe_4S_4Cl_4)$.[3]

All the procedures were performed under N_2. $FeCl_2$ anhydrous (1.4972 g, 11.8 mmol) was suspended in 60 mL of MeCN in a 200 mL of round bottom flask. Ph_4PCl (2.227 g, 5.9 mmol), NaSPh (2.2330 g, 17.7 mmol) and S (0.4745 g, 0.48 mmol) were added into the suspension with stirring. The obtained black reaction mixture was stirred at 25 °C for 2 hours and filtrated to remove dark brown residue. 300 mL of Et_2O was layered on the resultant black filtrate and kept for 2 days at 25 °C. The obtained black crystals were isolated by filtration and washed with Et_2O and dissolved in a minimum amount of MeCN and then recrystallized with Et_2O in the same manner. The recrystallized product was washed with Et_2O and dried under vacuum at 25 °C (51.0% yield).

Synthesis of *R*-BBI-*X* (*R* = Me, Et, Pr, Bu, *X* = I, Br).[4-5]

TAB (2.272 mg, 8.00 mmol) was dissolved in 80 mL of formic acid in a 300 mL of round bottom flask and the resultant solution was refluxed under N_2 flow for 3 days. The resultant brown solution was added with 40 mL of deionized water (DIW) and neutralized with K_2CO_3 at 0 °C. The resultant suspension was kept at 0 °C overnight. The off-white powder was isolated by filtration and washed with 40 mL of ice-cooled DIW and dried at 80°C under vacuum for 2 hours (bisbenzoimidazole: BBI, 90% yield). BBI (474.5 mg, 3.00 mmol) and NaH (239.9 mg, 6 mmol) were suspended in 100 mL of toluene in a 500 mL two-neck round bottom flask under N_2. The reaction mixture was refluxed for 2 hours under N_2 flow and cooled down to 25 °C. 18.0 mmol of alkyl halide (MeI, 1.12 mL; EtBr, 1.34 mL; PrBr, 1.64 mL; BuBr, 1.82 mL) was added with stirring and the resultant reaction mixture was refluxed for 2 hours. DMF (100 mL) was added after cooled down to 25 °C. The reaction mixture was heated at 110 °C overnight. Precipitation was completed by the addition of toluene after cooled down to 25 °C. The obtained solid product was isolated by filtration, washed with toluene and dried at 80 °C under vacuum for 2 hours (*R*-BBI-*X*, 51-79% yield). Me-BBI-I (500 MHz, DMSO-d_6): δH 9.92 (s, 2H), 8.84 (s, 2H), 4.19 (s, 12H). Et-BBI-Br (500 MHz, DMSO-d_6): δH 10.11 (s, 2H), 8.99 (s, 2H), 4.63 (m, J =7.2 Hz, 8H), 1.63 (t, J = 7.2 Hz, 12H). ^{n}Pr-BBI-Br (500 MHz, DMSO-d_6): δH 10.12 (s, 2H), 9.09 (s, 2H), 4.60 (t, J = 7.2 Hz, 8H), 2.03 (m, 8H), 0.98 (t, J = 7.2 Hz, 12H). ^{n}Bu-BBI-Br (500 MHz, DMSO-d_6): δH 10.01 (s, 2H), 8.96 (s, 2H), 4.59 (t, J = 7.2 Hz, 8H), 1.98 (m, 8H), 1.39 (m, 8H), 0.96 (t, J = 7.2 Hz, 12H).

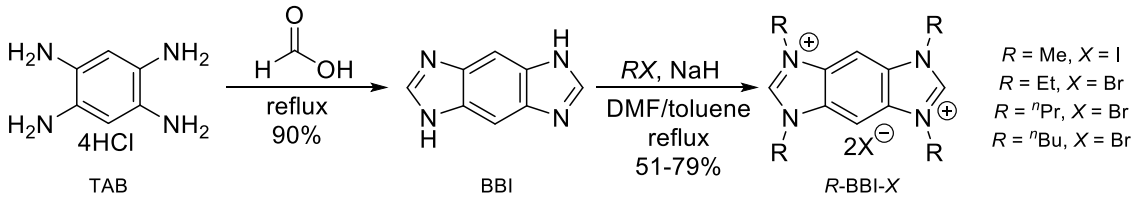
H2N
NH2
H2N
NH2
4HCl
TAB
O
H
OH
reflux
90%
N
H
N
H
N
BBI
RX, NaH
DMF/toluene
reflux
51-79%
R
N
N
R
2X
R = Me, X = I
R = Et, X = Br
R = nPr, X = Br
R = nBu, X = Br

R-BBI-X

Synthesis of [$Fe_4S_4Cl_2$(Me-NHC)] (1).

All the procedures were performed under N_2. 5 mL of DMF solution of Me-BBI-I (58.8 mg, 0.125 mmol) was mixed with 5 mL of DMF solution of Na^{t}BuO (24.0 mg, 0.25 mmol) at 25 °C for 25 min. The resultant deep red solution was added into 5 mL of DMF solution of $(PPh_4)_2(Fe_4S_4Cl_4)$ (29.3 mg, 0.025 mmol) with stirring in a 20 mL of Teflon-line vial and the reaction mixture was heated at 100 °C for 24 hours. The obtained black precipitate was isolated by centrifuge and washed with DMF (15 mL, 3 times) and DCM (10 mL, 3 times) and dried at 100 °C under vacuum for 3 hours (77-95% yield, Calcd for $C_{12}H_{14}Cl_2Fe_4N_4S_4$: C, 22.63; H, 2.22; N, 8.80. Found: C, 21.22; H, 2.45; 6.70.) The scale-up synthesis was performed in the same reaction scale and vial volume.

Controlled synthesis to vary the alkyl chains of NHC linkers.

The synthetic attempts varying the *R*-BBI-*X* (*R* = Et, ^{n}Pr, and ^{n}Bu; *X* = I) were carried out in the same manner as the above described procedure of **1**, and the products were denoted as **2-Et**, **3-^{n}Pr**, and **4-^{n}Bu**, respectively.

Table S1. Electrical conductivities of Fe and thiol-based CP/MOFs at room temperature.

Compounds	σ / S cm^{-1}	Method	Ref.
[Fe_4S_4]-based molecules and CP/MOFs			
[$Fe_4S_4Cl_2$(Me-NHC)] (**1**)	1.0×10^{-3}	Two-contact probe, pressed pellet	**This work**
[(PPh_4)$_2$($Fe_4S_4Cl_4$)]	1.0×10^{-10}	Two-contact probe, pressed pellet	This work
(TBA)$_2$[Fe_4S_4(SPh)$_4$]	$<1.0\times10^{-12}$	Two-contact probe, pressed pellet	6
(TMA)$_2$[Fe_4S_4(SPh)$_4$]	$<1.0\times10^{-12}$	Two-contact probe, pressed pellet	6
[(TMA)$_2$$Fe_4S_4(BDT)_2$], pristine	5.3×10^{-10}	Two-contact probe, pressed pellet	6
[(TMA)$_2$$Fe_4S_4(BDT)_2$], reduced	5.2×10^{-6}	Two-contact probe, pressed pellet	6
[(TMA)$_2$$Fe_4S_4(BDT)_2$], oxidized	7.1×10^{-10}	Two-contact probe, pressed pellet	6
[(TBA)$_2$$Fe_4S_4(BDT)_2$], pristine	3.3×10^{-11}	Two-contact probe, pressed pellet	6
[(TBA)$_2$$Fe_4S_4(BDT)_2$], reduced	6.2×10^{-9}	Two-contact probe, pressed pellet	6
[(TBA)$_2$$Fe_4S_4(BDT)_2$], oxidized	7.5×10^{-12}	Two-contact probe, pressed pellet	6
Fe and thiol-based CP/MOFs			
Fe_2(DSBDC) (DMF)$_2$	3.9×10^{-6}	Two-contact probe, pressed pellet	7
Fe_3(THT)$_2$(NH_4)$_3$	3.4×10^{-2}	Four-contact probe, film	8
Fe_3(PTC)	10	van der Pauw, pressed pellet	9
Fe_3(BHT)$_2$	0.68	Four-contact probe, film	10

PPh_4 = tetraphenylphosphonium. SPh = benzene thiolate. BDT= 1,4-benzenedithiolate. TMA = tetramethylammonium. TBA: tetrabutylammonium. H_4DSBDC = 2,5-disulfhydrylbenzene-1,4-dicarboxylic acid. THT = triphenylene-2,3,6,7,10,11-hexathiolate.

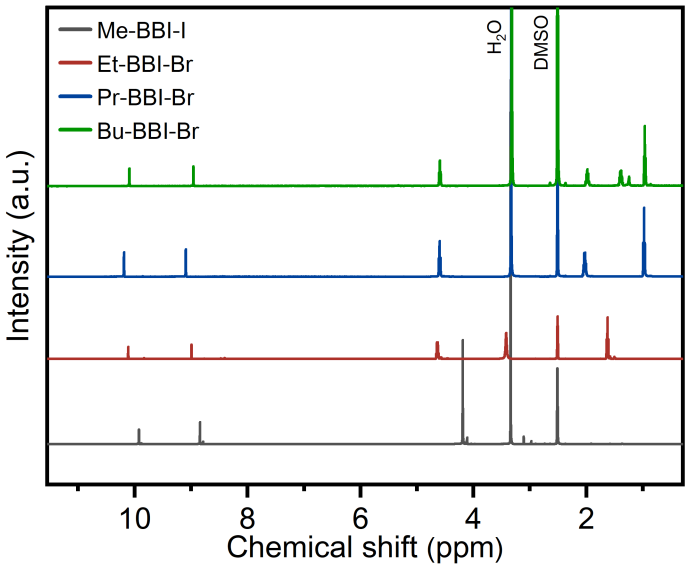

Figure S1. ^{1}H NMR of spectra of Me-BBI-I, Et-BBI-Br, Pr-BBI-Br, and Bu-BBI-Br in DMSO-d_6.

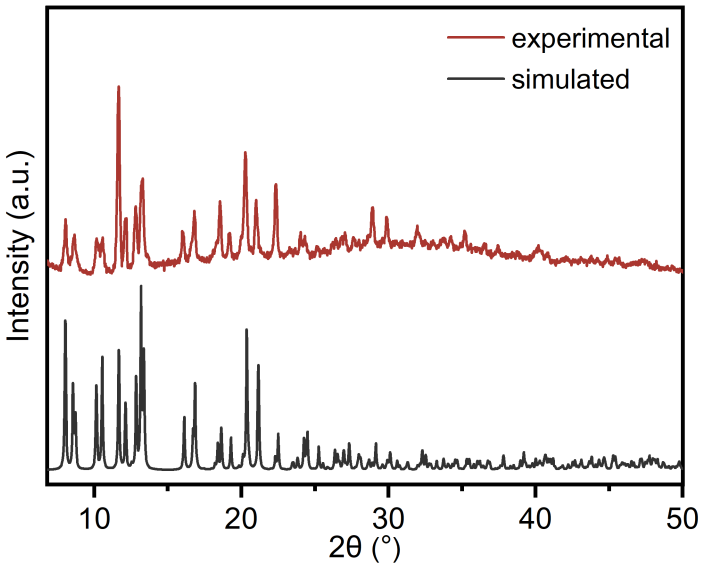

Figure S2. Simulated (black) and experimental (red) PXRD patterns of $(PPh_4)_2(Fe_4S_4Cl_4)$ under N_2. The differences in the relative intensities are due to the preferential orientation of the recrystallized particles.

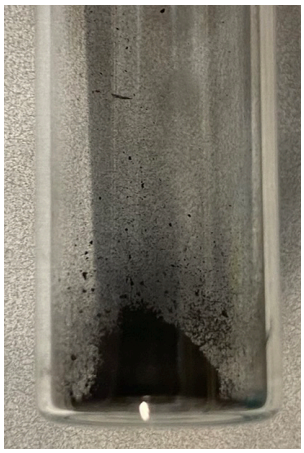

Figure S3. Image of the powder sample of **1**.

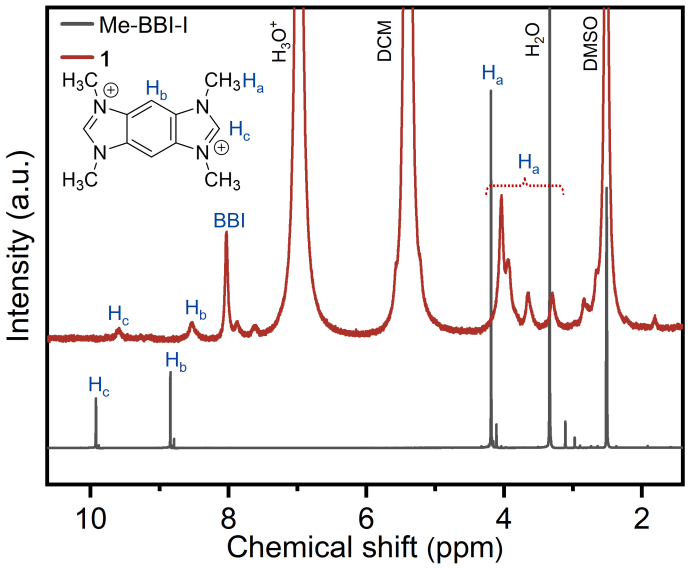

Figure S4. ^{1}H NMR spectra of **1** digested by DCl and Me-BBI-I in DMSO-d_6. The separated peaks of methyl groups (H_a) were due to the de-alkylation by DCl and BBI was formed as well.

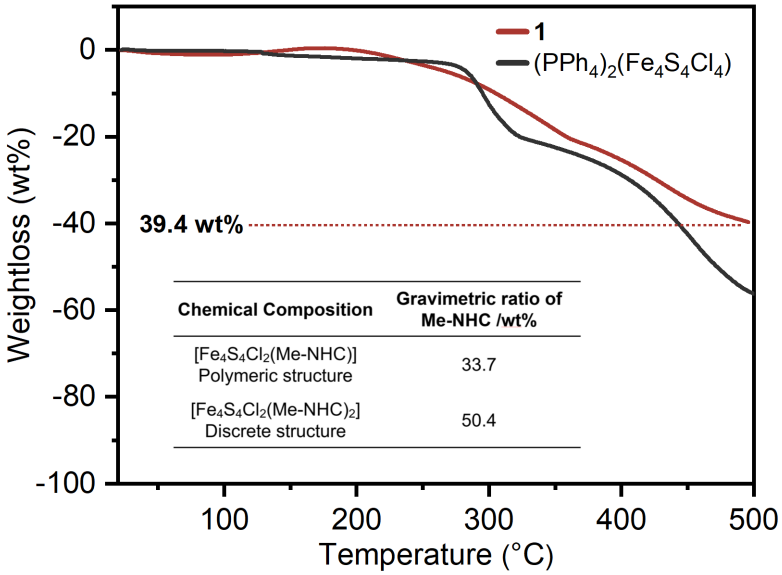

Figure S5. TGA profiles of **1** and $(PPh_4)_2(Fe_4S_4Cl_4)$ under N_2.

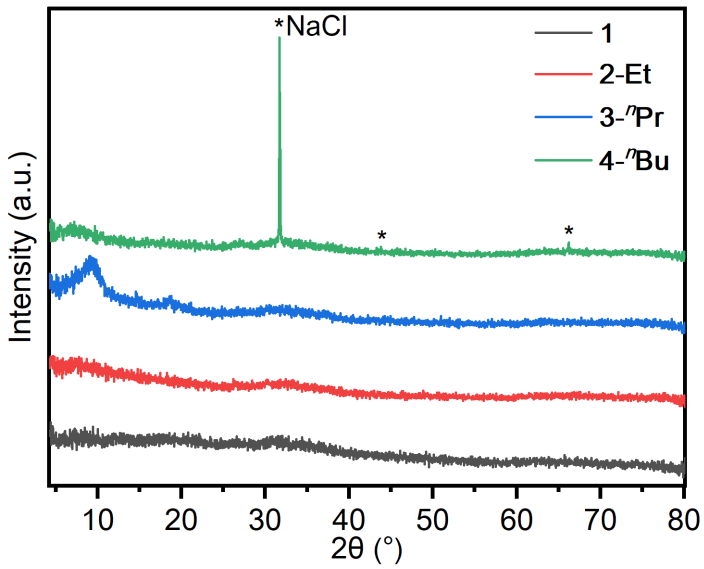

Figure S6. PXRD pattern of **1**, **2-Et**, **3-^{n}Pr**, and **4-^{n}Bu** under N_2. PXRD pattern of **4-^{n}Bu** was collected without washing with DMF due to the limited sample amount and NaCl as a by-product was observed.

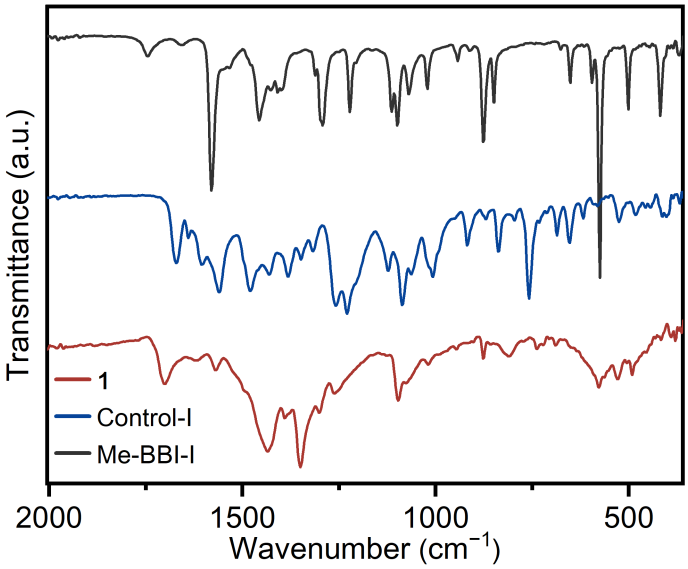

Figure S7. FT-IR spectra of **1**, control-I, and Me-BBI-I under N_2.

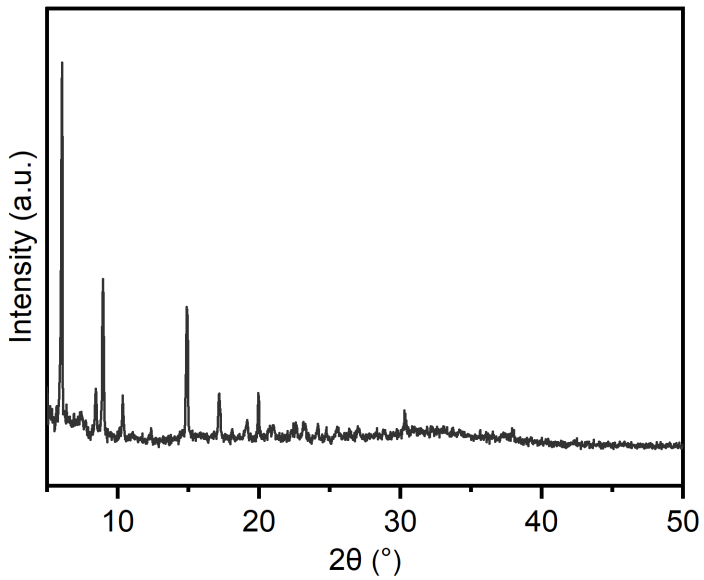

Figure S8. PXRD pattern of control-I under N_2.

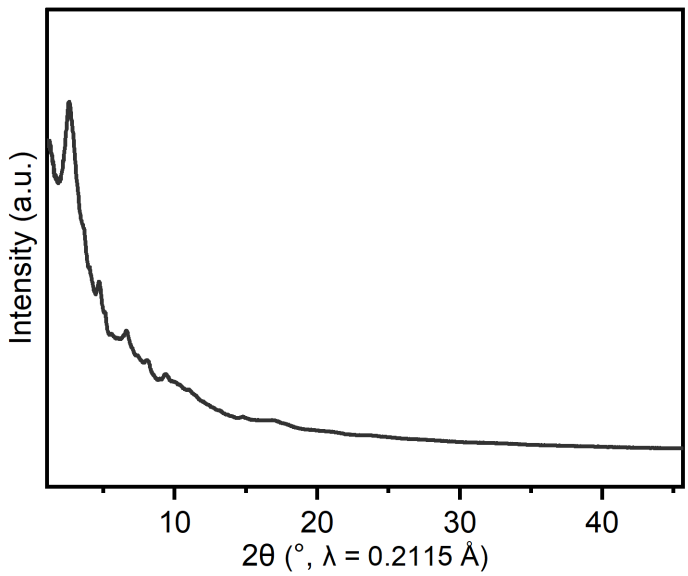

Figure S9. Synchrotron total X-ray scattering of **1**.

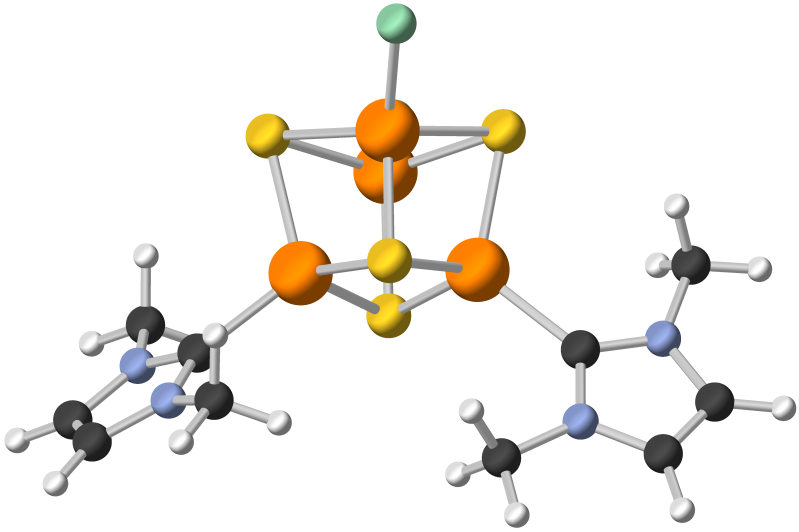

Figure S10. The model structure, $[Fe_4S_4Cl_2(MeNHC)_2]$ modified from $[Fe_4S_4Cl(mono\text{-}topic\ ^{i}Pr\text{-}NHC)_3]$ (CCDC code: HIYTUH). Fe: orange, S: yellow, Cl: green, N: blue, C: black, and H: white.

Table S2. Atom-atom correlations in the [Fe_4S_4] clusters reported in the CCDC database. The average correlation distances were obtained from the Crystal Maker.

CCDC code	Ligand	Bonding Fe-S / Å	Fe-Fe / Å	Diagonal Fe-S / Å
HIYVIX	NHC	2.288	2.720	3.884
HIYVUJ	NHC/CN	2.270	2.699	3.854
JAHXEW	CN	2.292	2.713	3.891
JOGLTA	NHC	2.330	2.680	3.930
JOTQAM	NHC	2.335	2.678	3.935
KAWVAG	CN	2.335	2.673	3.934
DEXXIN	Br	2.275	2.761	3.878
EAFEST	Cl	2.284	2.766	3.890
KAKFIL	I	2.675	2.753	3.876
KEWTAK	Cl	2.277	2.759	3.887
MEJZEJ	I	2.278	2.738	3.876
OTULEW	Cl	2.286	2.751	3.890
VAMFEU01	Cl	2.278	2.762	3.881

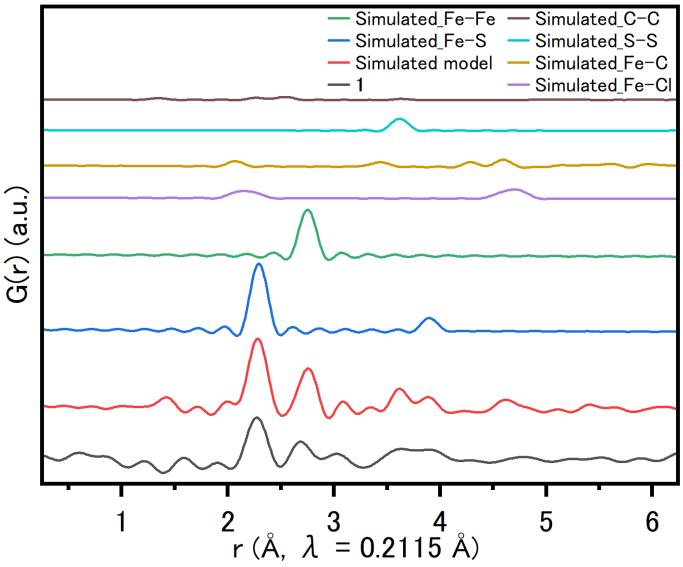

Figure S11. PDF profiles of **1** (black) and simulated model (red) and the simulated partial PDF fractions for the correlations of Fe-S (blue), Fe-Fe (green), Fe-Cl (purple), Fe-C (yellow), S-S (light blue), and C-C (brown).

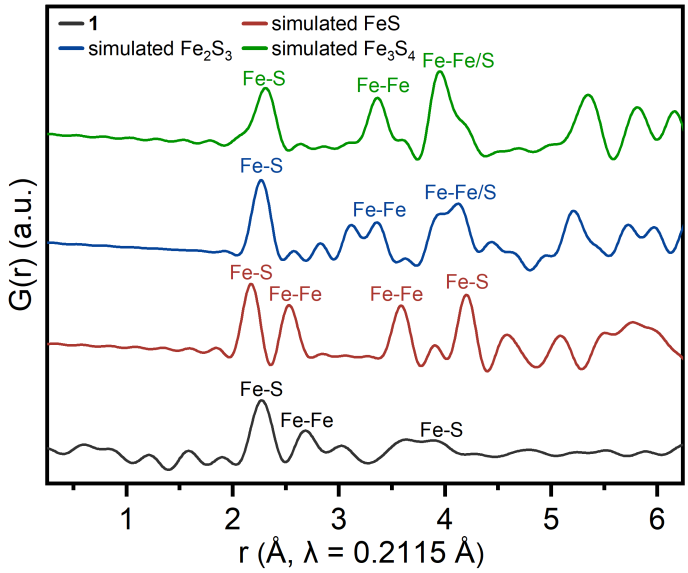

Figure S12. PDF profiles of **1**, simulated FeS (*P*4/*nmm*), Fe_3S_4 (*R*-3*c*), and Fe_2S_3 (*R*-3*c*). The representative atom-atom correlations are displayed, respectively.

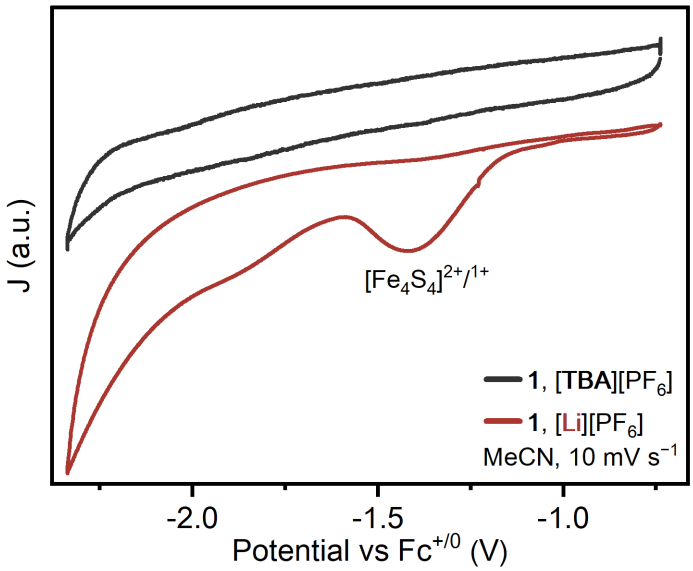

Figure S13. Solid-state CV of **1** deposited on the GC working electrode. 0.1 M of [TBA][PF_6] (black) or [Li][PF_6] (red) were used as a supporting electrolyte in acetonitrile.

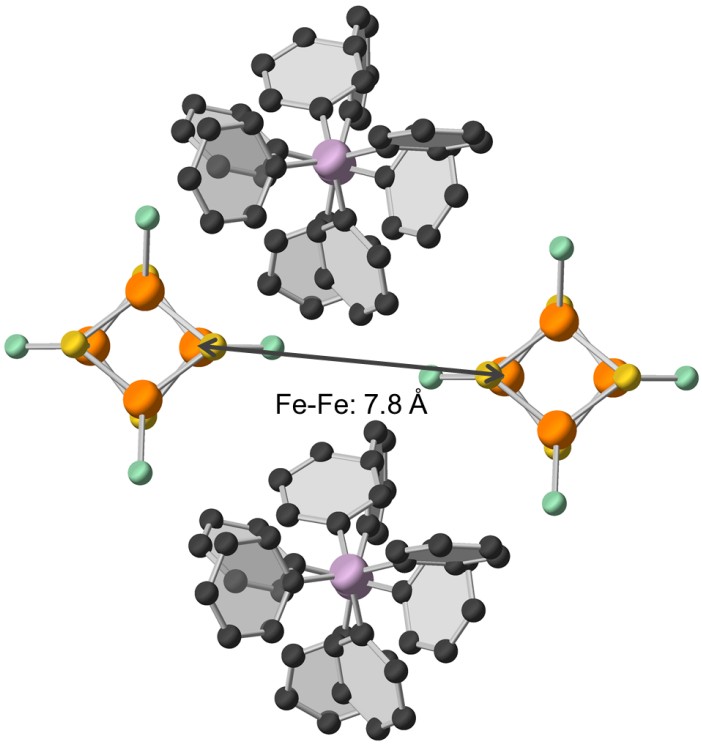

Figure S14. Isolation of $[Fe_4S_4]$ clusters by the bulky $[PPh_4]^+$ cations in $(PPh_4)_2(Fe_4S_4Cl_4)$. Fe: orange, S: yellow, Cl: green, P: purple, N: blue, and C: black. The hydrogen atoms are omitted for clarity.

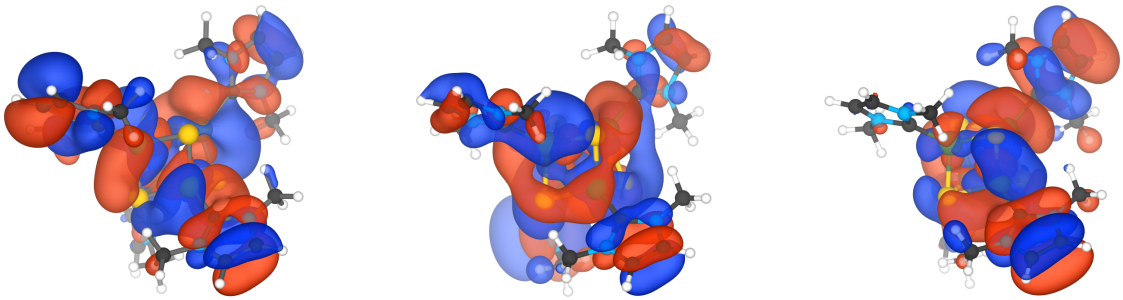

Figure S15. The degenerate singly occupied frontier orbitals of the NHC model cluster employed for DFT simulations plotted at isosurface values of 0.02.

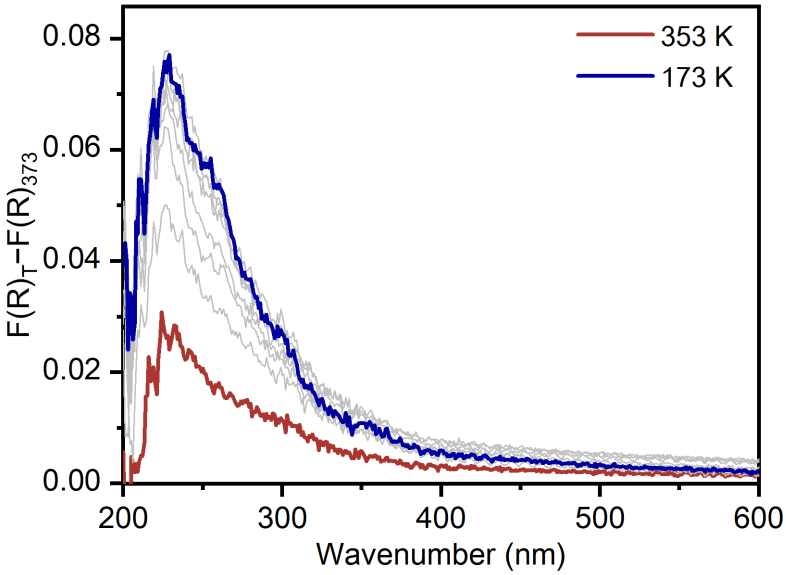

Figure S16. The plot of the difference curve, $\delta F(R)_T = F(R)_T - F(R)_{373}$, as a function of temperature.

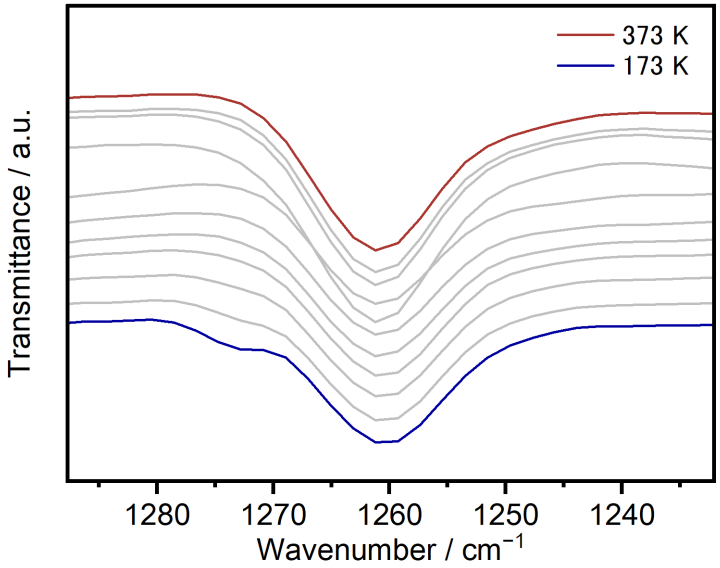

Figure S17. VT DRFITS of **1** in the temperature range of 173 and 373 K.

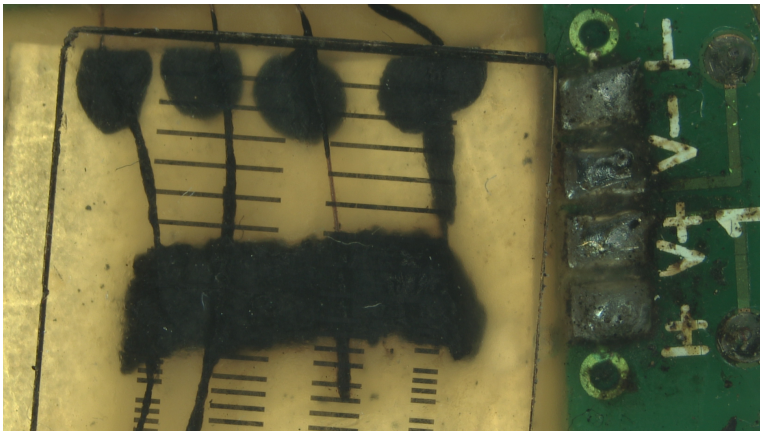

Figure S18. Image of the device for VT electrical conductivity by the four-contact probe, pressed pellet method.

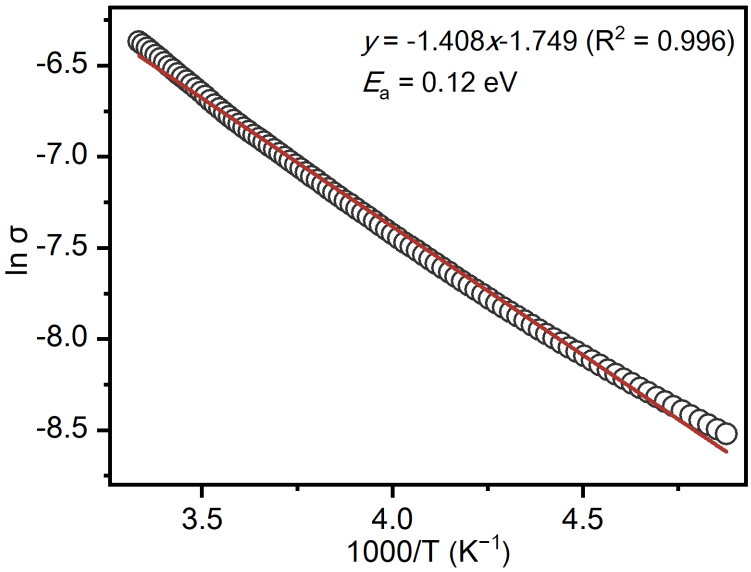

Figure S19. Arrhenius plot of the VT electrical conductivity of **1**.

Table S3. List of activation energies (E_a) of conductive CP/MOFs with conductivity of 10^{-1}−10 m S cm^{-1}.

Compounds	σ / mS cm^{-1}	E_a / eV	Method	Ref.
$[Fe_4S_4Cl_2(Me\text{-}NHC)]$ (**1**)	1.0	0.12	Two-contact probe, pressed pellet	**This work**
$[Cr_2(dbhq)_3][(H_2NMe_2)_{1.5}]$	1.2×10^{-1}	0.44	Two-contact probe, pressed pellet	[11]
$[Ti_2(Cl_2dhbq)_3][(H_2NMe_2)_2]$	2.7	0.27	Two-contact probe, pressed pellet	[11]
$Cu_3(HOTP)_2$	1.0×10^{-1}	0.24	Four-contact probe, film	[12]
$La_{1+x}(HOTP)$	8.2×10^{-1}	0.26	Two-contact probe, pressed pellet	[13]
$Nd_{1+x}(HOTP)$	8.0×10^{-1}	0.24	Two-contact probe, pressed pellet	[13]
$Yb_{1+x}(HOTP)$	10	0.25	Two-contact probe, pressed pellet	[13]
$Cd_2(TTFTB)$	2.9×10^{-1}	0.29	Two-contact probe, single crystal	[14]
$Cu[Ni(pdt)_2]$ oxidized by I_2	1.0×10^{-1}	0.18	Two-contact probe, film	[15]

dhbq = 2,5-dihydroxy-1,4-benzoquinone. Cl_2dhbq = 2,5-dichloro-3,6-dihydroxo-1,4-benzoquinone. HOTP = 2,3,6,7,10,11-hexaoxytriphenylene. pdt = 2,3-pyrazinedithiolene.

References

1. Juhás, P.; Davis, T.; Farrow, C. L.; Billinge, S. J. L., PDFgetX3: a rapid and highly automatable program for processing powder diffraction data into total scattering pair distribution functions. *J. Appl. Cryst.* **2013,** *46* (2), 560-566.

2. Farrow, C. L.; Juhas, P.; Liu, J. W.; Bryndin, D.; Božin, E. S.; Bloch, J.; Proffen, T.; Billinge, S. J. L., PDFfit2 and PDFgui: computer programs for studying nanostructure in crystals. *J. Phys. Cond. Matt.* **2007,** *19* (33), 335219.

3. Shim, Y.; Young, R. M.; Douvalis, A. P.; Dyar, S. M.; Yuhas, B. D.; Bakas, T.; Wasielewski, M. R.; Kanatzidis, M. G., Enhanced Photochemical Hydrogen Evolution from Fe_4S_4-Based Biomimetic Chalcogels Containing M^{2+} (M = Pt, Zn, Co, Ni, Sn) Centers. *J. Am. Chem. Soc.* **2014,** *136* (38), 13371-13380.

4. Kamplain, J. W.; Bielawski, C. W., Dynamic covalent polymers based upon carbene dimerization. *Chem. Commun.* **2006,** (16), 1727-9.

5. Guo, Z.; Song, N. R.; Moon, J. H.; Kim, M.; Jun, E. J.; Choi, J.; Lee, J. Y.; Bielawski, C. W.; Sessler, J. L.; Yoon, J., A benzobisimidazolium-based fluorescent and colorimetric chemosensor for CO_2. *J. Am. Chem. Soc.* **2012,** *134* (43), 17846-9.

6. Horwitz, N. E.; Xie, J.; Filatov, A. S.; Papoular, R. J.; Shepard, W. E.; Zee, D. Z.; Grahn, M. P.; Gilder, C.; Anderson, J. S., Redox-Active 1D Coordination Polymers of Iron-Sulfur Clusters. *J. Am. Chem. Soc.* **2019,** *141* (9), 3940-3951.

7. Sun, L.; Hendon, C. H.; Minier, M. A.; Walsh, A.; Dinca, M., Million-Fold Electrical Conductivity Enhancement in Fe2(DEBDC) versus Mn2(DEBDC) (E = S, O). *J. Am. Chem. Soc.* **2015,** *137* (19), 6164-7.

8. Dong, R.; Han, P.; Arora, H.; Ballabio, M.; Karakus, M.; Zhang, Z.; Shekhar, C.; Adler, P.; Petkov, P. S.; Erbe, A.; Mannsfeld, S. C. B.; Felser, C.; Heine, T.; Bonn, M.; Feng, X.; Canovas, E., High-mobility band-like charge transport in a semiconducting two-dimensional metal-organic framework. *Nat. Mater.* **2018,** *17* (11), 1027-1032.

9. Dong, R.; Zhang, Z.; Tranca, D. C.; Zhou, S.; Wang, M.; Adler, P.; Liao, Z.; Liu, F.; Sun, Y.; Shi, W.; Zhang, Z.; Zschech, E.; Mannsfeld, S. C. B.; Felser, C.; Feng, X., A coronene-based semiconducting two-dimensional metal-organic framework with ferromagnetic behavior. *Nat. Commun.* **2018,** *9* (1), 2637.

10. Tan, C. M.; Horikawa, M.; Fukui, N.; Maeda, H.; Sasaki, S.; Tsukagoshi, K.; Nishihara, H., Determination of Chemical Structure of Bis(dithiolato)iron Nanosheet. *Chem. Lett.* **2021,** *50* (4), 576-579.

11. Ziebel, M. E.; Darago, L. E.; Long, J. R., Control of Electronic Structure and Conductivity in Two-Dimensional Metal–Semiquinoid Frameworks of Titanium, Vanadium, and Chromium. *J. Am. Chem. Soc.* **2018**.

12. Rubio-Gimenez, V.; Galbiati, M.; Castells-Gil, J.; Almora-Barrios, N.; Navarro-Sanchez, J.; Escorcia-Ariza, G.; Mattera, M.; Arnold, T.; Rawle, J.; Tatay, S.; Coronado, E.; Marti-Gastaldo, C., Bottom-Up Fabrication of Semiconductive Metal-Organic Framework Ultrathin Films. *Adv. Mater.* **2018,** *30* (10).

13. Skorupskii, G.; Trump, B. A.; Kasel, T. W.; Brown, C. M.; Hendon, C. H.; Dinca, M., Efficient and tunable one-dimensional charge transport in layered lanthanide metal-organic frameworks. *Nat. Chem.* **2019**.

14. Sun, L.; Park, S. S.; Sheberla, D.; Dinca, M., Measuring and Reporting Electrical Conductivity in Metal-Organic Frameworks: Cd_2(TTFTB) as a Case Study. *J. Am. Chem. Soc.* **2016,** *138* (44), 14772-14782.

15. Kobayashi, Y.; Jacobs, B.; Allendorf, M. D.; Long, J. R., Conductivity, Doping, and Redox Chemistry of a Microporous Dithiolene-Based Metal−Organic Framework. *Chem. Mater.* **2010,** *22* (14), 4120-4122.